

Communication

Cubic Iron Core–Shell Nanoparticles Functionalized to Obtain High-Performance MRI Contrast Agents

Maria Volokhova ^{1,2}, Anna Shugai ¹, Masahiko Tsujimoto ³, Anna-Liisa Kubo ¹, Sven Telliskivi ⁴, Mait Nigul ⁵, Peep Uudeküll ¹, Heiki Vija ¹, Olesja M. Bondarenko ¹, Jasper Adamson ¹, Anne Kahru ¹, Raivo Stern ¹ and Liis Seinberg ^{1,*}

¹ National Institute of Chemical Physics and Biophysics, Akadeemia tee 23, 12618 Tallinn, Estonia; maria.volokhova@kbfi.ee (M.V.); anna.shugai@kbfi.ee (A.S.); anna-liisa.kubo@kbfi.ee (A.-L.K.); peep.uudekull@gmail.com (P.U.); heiki.vija@kbfi.ee (H.V.); olesja.bondarenko@kbfi.ee (O.M.B.); jasper.adamson@kbfi.ee (J.A.); anne.kahru@kbfi.ee (A.K.); raivo.stern@kbfi.ee (R.S.)

² Department of Chemistry and Biotechnology, Tallinn University of Technology, Akadeemia tee 15, 12618 Tallinn, Estonia

³ Institute for Integrated Cell-Materials Sciences, Kyoto University, Yoshida-Ushinomiya-cho, Sakyo-ku, Kyoto 606-8501, Japan; tsujimoto@icems.kyoto-u.ac.jp

⁴ North Estonia Medical Centre, 19 J. Sütiste tee, 13419 Tallinn, Estonia; s.telliskivi@gmail.com

⁵ The Radiology Clinic of Tartu University Hospital, 1a L. Puusepa St., 50406 Tartu, Estonia; mait.nigul@kliinikum.ee

* Correspondence: liis.seinberg@kbfi.ee



Citation: Volokhova, M.; Shugai, A.; Tsujimoto, M.; Kubo, A.-L.; Telliskivi, S.; Nigul, M.; Uudeküll, P.; Vija, H.; Bondarenko, O.M.; Adamson, J.; et al. Cubic Iron Core–Shell Nanoparticles Functionalized to Obtain High-Performance MRI Contrast Agents. *Materials* **2022**, *15*, 2228. <https://doi.org/10.3390/ma15062228>

Academic Editors: John Vakros, Evroula Hapeshi, Catia Cannilla and Giuseppe Bonura

Received: 21 February 2022

Accepted: 13 March 2022

Published: 17 March 2022

Publisher's Note: MDPI stays neutral with regard to jurisdictional claims in published maps and institutional affiliations.



Copyright: © 2022 by the authors. Licensee MDPI, Basel, Switzerland. This article is an open access article distributed under the terms and conditions of the Creative Commons Attribution (CC BY) license (<https://creativecommons.org/licenses/by/4.0/>).

Abstract: Nanoparticles with SiO₂ coating were synthesized to have a cubic iron core. These were found to have saturation magnetization very close to the highest possible value of any iron-containing nanoparticles and the bulk iron saturation magnetization. The in vitro toxicology studies show that they are highly biocompatible and possess better MRI contrast agent potential than iron oxide NPs.

Keywords: nanomaterials; synthesis; magnetic properties; MRI contrast agents; toxicity; ROS

1. Introduction

There has been considerable interest in magnetic nanoparticles (NPs) over recent decades due to their use in pharmaceutical and biomedical applications, including drug delivery [1], hyperthermia treatment [2,3] and magnetic resonance imaging (MRI) [4–6]. The most developed of these fields is the use of superparamagnetic iron oxide nanoparticles (SPIONs) as T₂-negative contrast-enhancing agents in MRI [5,7]. Multiple aspects, including biocompatibility, size, shape, charge and magnetic properties of the NPs, need to be taken into account when developing the most efficient NPs for use in high-performance MRI measurement [5–8]. SPIONs are efficient in lowering the transverse relaxation time (T₂) of water proton spins in tissues. This process is described by relaxivity, r₂, given by the equation

$$\frac{1}{T_{2,m}} = r_2 * C_m$$

where C_m is the total concentration of magnetic ions [9]. The total relaxation rate is then given by the equation

$$\frac{1}{T_2} = \frac{1}{T_{2,0}} + \frac{1}{T_{2,m}}$$

where 1/T_{2,0} is the relaxation rate in the absence of magnetic NPs. Accordingly, for the lowest T₂ relaxation time of proton spins, high r₂ values are desired. One downside of SPIONs is that their saturation magnetization (M_s) is clearly below that of bulk iron. Typically, investigated SPIONs, magnetite (Fe₃O₄) and its oxidized form maghemite (γ-Fe₂O₃), have M_s values of 124 emu per g-Fe and 109 emu per g-Fe, respectively [10]. Metallic iron's

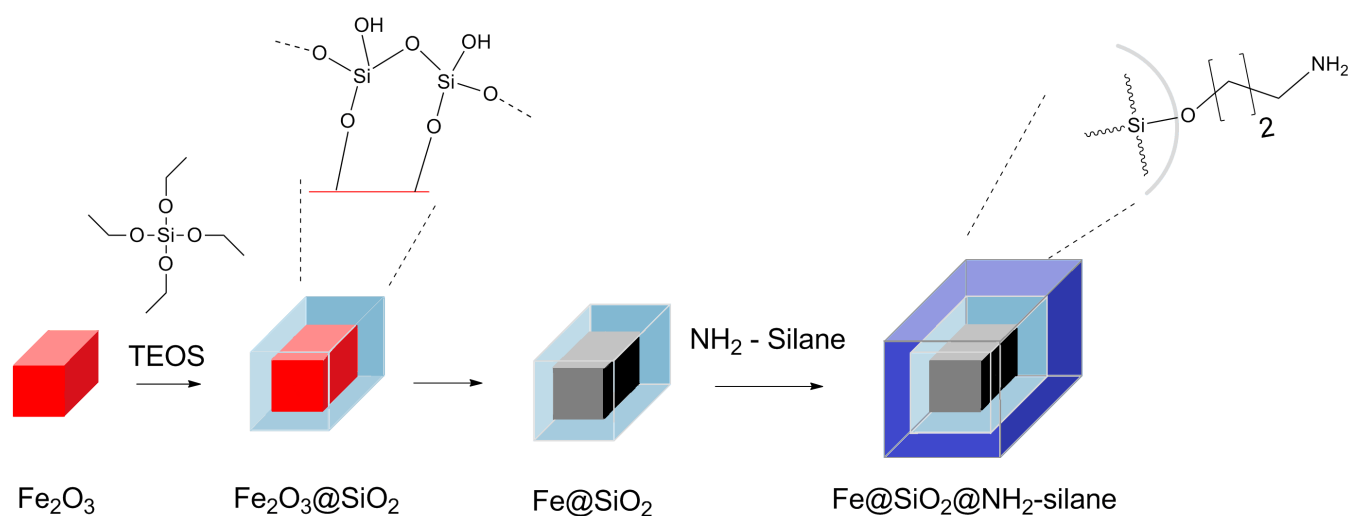
(α -Fe) saturation magnetization of 218 emu per g-Fe exceeds these numbers nearly twofold. From the perspective of MRI, high M_s values are crucial for MRI signal enhancement since contrast agents with high M_s increase the relaxation rate of proton spins according to $1/T_2, m \propto M_s^2$ [11]. Therefore, based on increased M_s , metallic α -Fe NPs have potential to produce better quality images for high-performance MRI [8]. The latter argument has prompted this study, where we synthesize and investigate NPs with a metallic cubic iron core. Solution-based synthesis of spherical α -Fe NPs with cPEG coating was performed by the optimized chemical reduction of ferrous chloride with sodium borohydride [3]. Another study on PEGylated Fe@Fe₃O₄NPs showed that they are a promising MRI contrast agent [12]. Additionally, iron NPs with TRITC–dextran coating (size <20 nm) were synthesized using cryomill and with saturation magnetization (180 per g-Fe) [13].

Herein, we focus on solid state synthesis of α -Fe NPs and their MRI relaxivity measurements. Traditionally, in solid state, the preparation method for spherical SiO₂-coated α -Fe NPs is carried out via reduction of spherical SiO₂-coated iron oxide NPs with H₂ gas under high temperature [14,15]. Recently, Yamamoto et al. used CaH₂ as a reducing agent for the synthesis of spherical α -Fe NPs and lowered the reduction working temperature down to 20–300 °C [16]. They later demonstrated this reduction method to be applicable for spherical α -Fe@SiO₂ NP synthesis from spherical Fe₃O₄@SiO₂ NPs [8,17]. Furthermore, saturation magnetization of the spherical SiO₂-coated Fe nanoparticles increased with decreasing SiO₂ thickness [17]. Herein, we apply this reduction method on cubic core α -Fe₂O₃@SiO₂ to obtain α -Fe@SiO₂ NPs with an unusual cubic core morphology and furthermore characterize their magnetic and relaxation properties on a clinical 3.0 T MRI instrument. Cubic shape is important due to the change in the magnetic properties and lower saturation magnetization could expand the application to T1 or a dual mode contrast agent. For biomedical applications, NPs with biocompatible shells, e.g., coated by inert inorganic materials (such as SiO₂ shell) or various hydrophilic polymers (such as albumin, polyethylene glycol) are desirable [6,18]. Coating α -Fe NPs has a further advantage of stabilizing the NPs against oxidation as their magnetic properties are altered when oxidation occurs. Further, coating of the NPs with silane moieties has shown improvement of NP colloidal stability and additionally provides ample opportunities to decorate the NP surface with functional molecules [8].

Moreover, an NH₂-silane coating can render the NPs dispersible in aqueous solutions over a wide pH range [19], link to biomolecules, including applications in DNA and RNA purification [20] and enhance cellular uptake of the NPs without increased cytotoxicity [21].

The generation of reactive oxygen species (ROS) has been proposed as the main mechanism behind the adverse effects of iron oxide NPs [18,22]. Uncoated iron oxide NPs are usually significantly more toxic than coated NPs because Fe ions are efficient inducers of ROS production. In addition, the surface of NPs can contribute into catalytic ROS production by amplifying the role of chemical reactions occurring at the surface [23], while the coating functions as a barrier to reduce the toxicity [24]. While some authors reported no or low toxicity even for uncoated iron oxide NPs to various human cell lines and primary human cells in vitro [25–27], others demonstrated moderate toxicity, e.g., toxicity at exposure concentrations below 100 mg/L [22,28].

Firstly, we report the synthesis of SiO₂-coated iron metal core (α -Fe@SiO₂) NPs with a cubic morphology (Scheme 1). Secondly, we characterize the cubic core/shell NPs' magnetic properties and show that they possess enhanced MRI relaxivity as compared to their iron oxide counterparts (γ -Fe₂O₃@SiO₂). Thirdly, we functionalize the α -Fe@SiO₂ NPs with 3-aminopropyltrimethoxysilane (α -Fe@SiO₂@NH₂-silane) and, finally, perform nanotoxicology studies to demonstrate their low cytotoxicity.

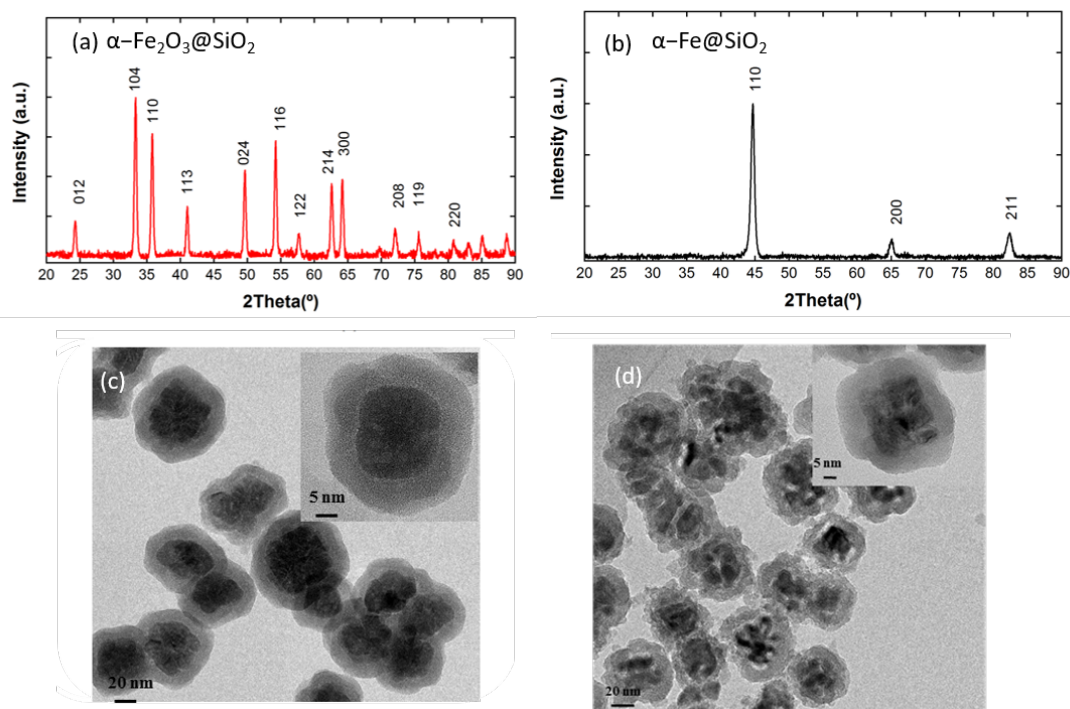


Scheme 1. SiO₂-coated α -Fe@SiO₂ cubic NP synthesis schema and their further functionalization.

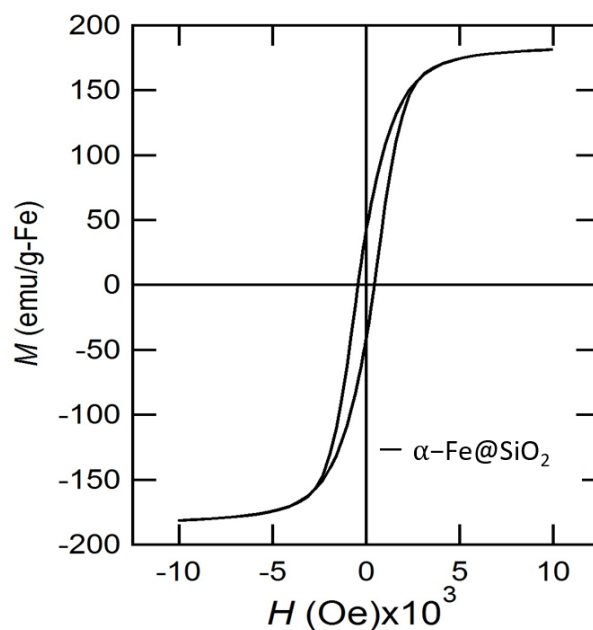
2. Results and Discussion

Described below are experimental details, which have been limited to the requisite minimum. Further details are presented in Supplementary Materials (SM). Monodispersed cubic α -Fe₂O₃ NPs were synthesized by a facile one-step solvothermal route from ferric nitrite [Fe(NO₃)₃·9H₂O], *N,N*-dimethyl formamide (DMF) and poly(*N*-vinyl-2-pyrrolidone) up to 200 °C [29,30]. The crystallographic structure of the NPs was confirmed by powder X-ray diffraction (PXRD) analysis, shown in Scheme 2a. The PXRD pattern revealed the hematite phase of iron oxide with characteristic reflections at 24.1°, 33.2°, 35.6°, 40.8°, 49.5°, 54.1°, 62.5° and 64.0° with the Miller indexes closest matching peak locations of hematite iron oxide phase PDF card 033-0664 from the ICDD PDF-2 database. The NPs with a cubic core shape and with the cube's edge were observed to be 40 nm using transmission electron microscope (TEM) analysis (Scheme 2c). The NPs were then coated with a SiO₂ layer via a modification of the method published by Yamamoto et al. TEM images confirm the SiO₂ coating thickness to be 10 nm on average (Scheme 2c).

Subsequently, the cubic core shape α -Fe₂O₃@SiO₂ NPs were subject to reduction with CaH₂ to obtain SiO₂-coated α -Fe@SiO₂ NPs (Scheme 2d). The reduction reaction was a modification of the procedure described by Yamamoto recently [16]. The NP and CaH₂ mixture was heated at 260 °C for 4 days (for a detailed description, see the SM). The color of the reaction mixture changed from orange-red to black, indicating the formation of metal iron Fe⁰. The structure of the pure metallic body-centered-cubic (bcc) α -Fe core was confirmed by PXRD analysis (Scheme 2b) with 110, 200 and 211 peaks indexed [16]. TEM images in Scheme 2d reveal voids in the reduced NPs due to oxygen leaving the iron oxide NPs upon reduction. Therefore, the morphology of the as-synthesized NPs could be referred to as quasi- or pseudo-cubic core. We then characterized the NPs' magnetic properties with PPMS (Quantum Design) magnetometry after exposure to air for 7 days. The M_s value for the nanoparticles was 180 emu per g-Fe (Scheme 3). The obtained saturation magnetization is nearly twice as large as for commercial SPION contrast agent Resovist (95 emu per g-Fe) and close to that of bulk iron (218 emu per g-Fe) [31].



Scheme 2. (a) PXRD patterns of α -Fe₂O₃@SiO₂ and (b) α -Fe@SiO₂ after CaH₂ reduction reaction of α -Fe₂O₃@SiO₂. (c) TEM images obtained from α -Fe₂O₃@SiO₂ nanocubes and (d) from α -Fe@SiO₂ nanocubes.

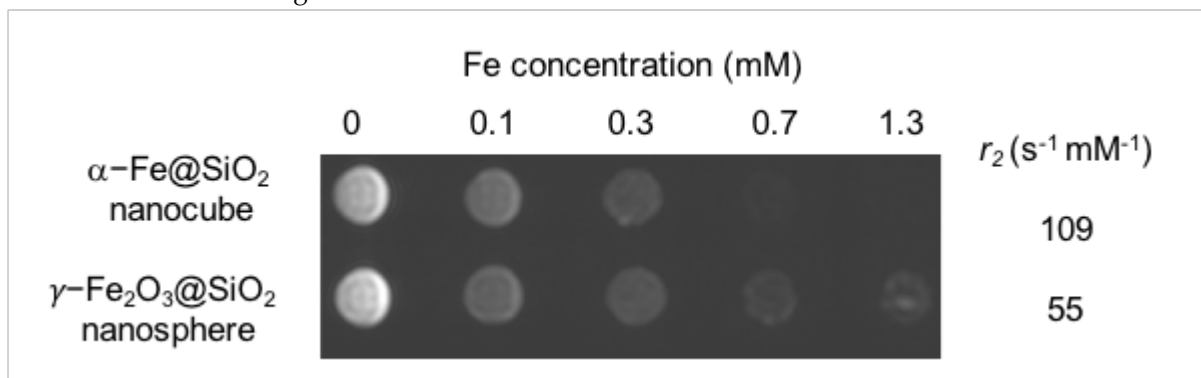


Scheme 3. Magnetic hysteresis curve of cubic core α -Fe@SiO₂ showing the saturation magnetization of 180 emu/g-Fe.

The mass fraction of α -Fe in the SiO₂-coated cubic core NPs was found to be 33% by using total reflection X-ray fluorescence spectroscopy (TRXF) Picofox S2 and elemental analysis as described in the SM. This value was used to calculate the mass of iron in the NPs for MRI measurements reported in this paper (details below). The mass fraction of iron for spherical maghemite (γ -Fe₂O₃@SiO₂) was found to be 27% using the same methods.

The surface of the SiO₂-coated iron NPs was further modified with 3-aminopropyltriethoxy-silane (NH₂-silane) for additional decoration with functional molecules, such as albumin. The NH₂-silane coating was successfully implemented as confirmed with Fourier transform infrared (FTIR) spectroscopy (Scheme S1 in SM). The transverse relaxivity (r_2) of the as-synthesized cubic core α -Fe@SiO₂ NPs was tested with a clinical 3.0 T Philips Achieve MRI scanner. As reference compounds, commercially available spherical maghemite coated with SiO₂ (γ -Fe₂O₃@SiO₂) was used (the latter structure is confirmed by PXRD analysis in Scheme S2). SiO₂ coating was implemented with the same procedure as described above. γ -Fe₂O₃@SiO₂ NPs had a core diameter of 60 nm (TEM images are shown in Scheme S2).

The obtained r_2 values were 55 s⁻¹mM⁻¹ for spherical γ -Fe₂O₃@SiO₂, and 109 s⁻¹mM⁻¹ for cubic core α -Fe@SiO₂ (Scheme 4). The results show that pure metal α -Fe@SiO₂ NPs have nearly twice as high r_2 relaxivity compared to maghemite NPs. This finding can be attributed to the larger M_s values of pure metal NPs. The literature r_2 values of iron oxides magnetite and maghemite vary according to particle size and the size of the polymer shell. In general, larger NPs have enhanced r_2 relaxivity and, depending on the study, the values for spherical SPIONs range from as little as 13 s⁻¹mM⁻¹ to 385 s⁻¹mM⁻¹ [11,32]. Nevertheless, in our study, α -Fe NPs showed clearly enhanced MRI relaxivity compared to maghemite NPs.

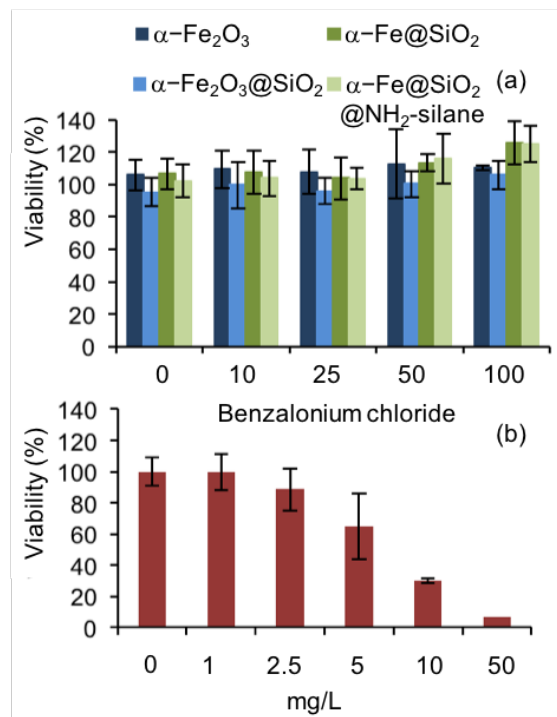


Scheme 4. T₂ weighted contrast MRI image of α -Fe@SiO₂ nanocubes and γ -Fe₂O₃@SiO₂ nanospheres with increasing Fe concentrations and their r_2 values measured by 3.0 T clinical MRI system.

Dynamic light scattering studies revealed the average hydrodynamic size (D_h) of NPs to be 100–200 nm for α -Fe₂O₃ and α -Fe₂O₃@SiO₂, 200–400 nm for α -Fe@SiO₂ and 600–800 nm for α -Fe@SiO₂@NH₂-silane in Milli-Q (MQ) water as well in the toxicity testing medium (see SM Table S1). D_h of NPs was larger than the primary core with the SiO₂ shell size determined by TEM. The polydispersity index (PDI) of NPs was between 0.07 and 0.31 (SM Table S1), showing the monodispersity and stability of NP solutions. Subsequently, cytotoxicity characterization was performed on the series of synthesized NPs shown in Scheme 1. To assess the possible adverse effects of NPs on living cells, an in vitro toxicity assay with the HepG2 cell line in vitro was performed (for details see SM).

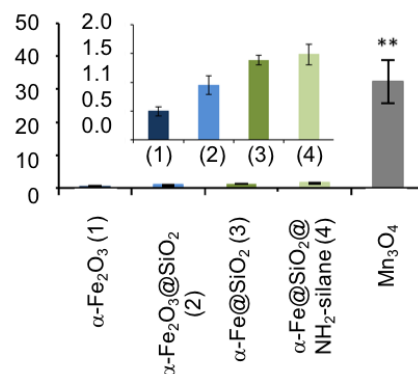
HepG2, the model for human liver cells in vitro, was chosen since liver is the primary target organ of xenobiotics and is the major accumulation site for Fe-based NPs [33]. While the toxic chemical benzalkonium chloride (a chosen positive control) remarkably reduced the viability of HepG2 cells at 5 mg/L, none of the tested NPs exhibited toxicity at the highest concentration tested (100 mg/L) (Scheme 5). According to the literature, the toxicity data on the adverse effect of iron oxide NPs on human cell lines in vitro are heterogeneous and depend on the NP type and functionalization, tested cell lines and toxicity endpoint used. However, shedding of Fe ions from NP cores may induce the production of excessive ROS that may lead to cytotoxicity or/and oxidative DNA damage and genotoxicity. In the case of cytotoxicity, the mechanism of action of iron oxide NPs has been associated with ROS and resulting oxidative damage [22]. Therefore, we then assessed the possible

sub-toxic adverse effects of synthesized NPs and measured the induction of abiotic ROS using H₂DCFDA, a ROS-sensitive fluorescent probe (see the SM).



Scheme 5. Viability of HepG2 cells in vitro determined by Resazurin assay after 24 h exposure to cubic core Fe nanoparticles (a) or benzalkonium chloride (b). Average from three independent experiments with standard deviation is shown.

While ROS-generating Mn₃O₄ NPs induced remarkable ROS at concentrations of 100 mg/L, none of tested Fe NPs caused the production of abiotic ROS at the highest concentration (100 mg/L) tested (Scheme 6). Therefore, the used toxicity test and abiotic ROS assay revealed that under the conditions used, the synthesized NPs showed no evidence of nanotoxicity up to a high concentration, 100 mg/L, making them promising candidates for further biocompatibility studies and biomedical applications. The upper limit value of the concentration used in the nanotoxicology research is sufficient for an MRI study.



Scheme 6. Induction of abiotic ROS with four different Fe NPs and Mn₃O₄ NPs (a positive control) [34] measured at a concentration of 100 mg/L using 2',7'-dichlorofluorescein diacetate (H₂DCFDA) assay after a 45 min incubation. Average from three independent experiments with standard deviation is shown; ** $p < 0.01$. The inset is a zoomed-in view of the synthesized NPs.

3. Conclusions

In conclusion, we have synthesized cubic core α -Fe NPs with a SiO₂ coating and further organic functionalization with NH₂-silane. The cubic core α -Fe NPs' M_s value of as much as 180 emu per g-Fe is quite close to that of bulk iron, 218 emu per g-Fe, and results in high MRI relaxivity r_2 . We have indeed determined that the cubic core α -Fe NPs' r_2 value was larger than for maghemite NPs, 109 s⁻¹mM⁻¹ compared to 55 s⁻¹mM⁻¹. Furthermore, cytotoxicity studies showed that the synthesized NPs were not toxic to liver cells in vitro even at 100 mg/L, revealing them to be biocompatible.

Supplementary Materials: The following supporting information can be downloaded at: <https://www.mdpi.com/article/10.3390/ma15062228/s1>, Scheme S1: IR spectra of α -Fe@SiO₂ cubic nanoparticles before (black) and after (blue) coating with NH₂-silane; Scheme S2: (a) Powder XRD patterns of γ -Fe₂O₃@SiO₂ and (b) TEM image of γ -Fe₂O₃@SiO₂; Table S1: Summary on characterization of cubic Fe nanoparticles used in the current study.

Author Contributions: L.S. designed and directed the study; M.V., P.U. and L.S., carried out the synthesis, powder X-ray measurement and characterization; R.S. helped with the PPMS measurement and data analysis; A.S. and L.S. carried out IR-FT spectroscopy measurement and analysis; A.-L.K. and O.M.B. carried out toxicology studies; M.T. carried out TEM and HRTEM characterization and analysis; H.V. carried out the element analysis measurements; M.N., S.T., J.A., H.V. and L.S. carried out and helped with clinical MRI measurements and data analysis; L.S., M.V., R.S., J.A., O.M.B., A.-L.K. and A.K. wrote the manuscript with contribution from all the authors. All authors have read and agreed to the published version of the manuscript.

Funding: This research was funded by the Estonian Ministry of Education and Research grants number IUT23-3, IUT23-7, IUT23-5, PUT1046, PUT210, PUT1015, and PRG4, and by the European Regional Development Fund projects no TK133 and TK134.

Institutional Review Board Statement: Not applicable.

Informed Consent Statement: Not applicable.

Data Availability Statement: The data presented in this study are available on request from the corresponding author.

Acknowledgments: Research was sponsored by the institutional research funding IUT23-3, IUT23-7, IUT23-5, PUT1046, PUT210, PUT1015 and PRG4 of the Estonian Ministry of Education and Research, grant ArengufondOB from the Development Fund of the National Institute of Chemical Physics and Biophysics and the European Regional Development Fund project no TK134. We are grateful to Heiti Kender assistance with MRI measurements.

Conflicts of Interest: The authors declare no conflict of interest.

References

1. Mura, S.; Nicolas, J.; Couvreur, P. Stimuli-responsive nanocarriers for drug delivery. *Nat. Mater.* **2013**, *12*, 991–1003. [[CrossRef](#)] [[PubMed](#)]
2. Martinez-Boubeta, C.; Simeonidis, K.; Makridis, A.; Angelakeris, M.; Iglesias, O.; Guardia, P.; Cabot, A.; Yedra, L.; Estradé, S.; Peiró, F.; et al. Learning from Nature to Improve the Heat Generation of Iron-Oxide Nanoparticles for Magnetic Hyperthermia Applications. *Sci. Rep.* **2013**, *3*, 1652–1660. [[CrossRef](#)]
3. Hadjipanayis, C.G.; Bonder, M.J.; Balakrishnan, S.; Wang, X.; Mao, H.; Hadjipanayis, G.C. Metallic Iron Nanoparticles for MRI Contrast Enhancement and Local Hyperthermia. *Small* **2008**, *4*, 1925–1929. [[CrossRef](#)] [[PubMed](#)]
4. Kircher, M.F.; de la Zerda, A.; Jokerst, J.V.; Zavaleta, C.L.; Kempen, P.J.; Mittra, E.; Pitter, K.; Huang, R.; Campos, C.; Habte, F. A brain tumor molecular imaging strategy using a new triple-modality MRI-photoacoustic-Raman nanoparticle. *Nat. Med.* **2012**, *18*, 829–834. [[CrossRef](#)] [[PubMed](#)]
5. Zhou, Z.Z.; Bao, J.; Wang, Z.; Hu, J.; Chi, X.; Ni, K.; Wang, R.; Chen, X.; Chen, Z.; Gao, J. Octapod iron oxide nanoparticles as high-performance T₂ contrast agents for magnetic resonance imaging. *Nat. Commun.* **2013**, *4*, 2266–2273.
6. Weissleder, R.; Nahrendorf, M.; Pittet, M.J. Imaging macrophages with nanoparticles. *Nat. Mater.* **2014**, *13*, 125–138. [[CrossRef](#)]
7. Li, L.; Jiang, W.; Luo, K.; Song, H.; Lan, F.; Wu, Y.; Gu, Z. Superparamagnetic Iron Oxide Nanoparticles as MRI contrast agents for Non-invasive Stem Cell Labeling and Tracking. *Theranostics* **2013**, *3*, 595–615. [[CrossRef](#)]

8. Kohara, K.; Yamamoto, S.; Seinberg, L.; Murakami, T.; Tsujimoto, M.; Ogawa, T.; Kurata, H.; Kageyama, H.; Takano, M. Carboxylated SiO₂-coated α -Fe nanoparticles: Towards a versatile platform for biomedical applications. *Chem. Commun.* **2013**, *49*, 2566–2573. [[CrossRef](#)]
9. Merbach, A.S.; Helm, L.; Tóth, E. *The Chemistry of Contrast Agents in Medical Magnetic Resonance Imaging*; Wiley: Hoboken, NJ, USA, 2001.
10. Huber, D.L. Synthesis, Properties, and Applications of Iron Nanoparticles. *Small* **2005**, *1*, 482–501.
11. Tong, S.; Hou, S.; Zheng, Z.; Zhou, J.; Bao, G. Coating optimization of superparamagnetic iron oxide nanoparticles for high T2 relaxivity. *Nano Lett.* **2010**, *10*, 4607–4613. [[CrossRef](#)]
12. Zhou, Z.; Sun, Y.; Shen, J.; Wei, J.; Yu, C.; Kong, B.; Liu, W.; Yang, H.; Yang, S.; Wang, W. Iron/iron oxide core/shell nanoparticles for magnetic targeting MRI and near-infrared photothermal therapy. *Biomaterials* **2014**, *35*, 7470–7478. [[CrossRef](#)] [[PubMed](#)]
13. Tiwary, C.S.; Mudakavi, R.J.; Kishore, S.; Kashyap, S.; Elumalai, R.; Chakravorty, D.; Raichurac, A.M.; Chattopadhyay, K. Magnetic iron nanoparticles for in vivo targeted delivery and as biocompatible contrast agents. *RSC Adv.* **2016**, *6*, 114344–114352. [[CrossRef](#)]
14. Tartaj, P.; Serna, C.J. Synthesis of Monodisperse Superparamagnetic Fe/Silica Nanospherical Composites. *J. Am. Chem. Soc.* **2003**, *125*, 15754–15755. [[CrossRef](#)] [[PubMed](#)]
15. Zhu, J.; Wei, S.; Lee, I.Y.; Park, S.; Willis, J.; Haldolaarachchige, N.; Young, D.P.; Luo, Z.; Guo, Z. Silica stabilized iron particles toward anti-corrosion magnetic polyurethane nanocomposites. *Rsc Adv.* **2012**, *2*, 1136–1143. [[CrossRef](#)]
16. Yamamoto, S.; Ruwan, G.; Tamada, Y.; Kohara, K.; Kusano, Y.; Sasano, T.; Ohno, K.; Tsujii, Y.; Kageyama, H.; Ono, T. Transformation of Nano- to Mesosized Iron Oxide Cores to α -Fe within Organic Shells Preserved Intact. *Chem. Mater.* **2011**, *23*, 1564–1569. [[CrossRef](#)]
17. Matsumoto, A.; Sugiura, T.; Kobashi, M.; Yamamoto, S. Preparation and Magnetic Properties of Nano-Sized Iron Powder Particles Coated with Silica Film by Calcium Hydride Reduction Method. *Mater. Trans.* **2020**, *61*, 1404–1408. [[CrossRef](#)]
18. Mahmoudi, M.; Sant, S.; Wang, B.; Laurent, S.; Sen, T. Superparamagnetic iron oxide nanoparticles (SPIONs): Development, surface modification and applications in chemotherapy. *Adv. Drug Deliv. Rev.* **2011**, *63*, 24–46. [[CrossRef](#)]
19. Palma, R.D.; Peeters, S.; Bael, M.J.V.; den Rul, H.V.; Bonroy, K.; Laureyn, W.; Mullens, J.; Borghs, G.; Maes, G. Silane ligand exchange to make hydrophobic superparamagnetic nanoparticles water-dispersible. *Chem. Mater.* **2007**, *19*, 1821–1831. [[CrossRef](#)]
20. Ma, M.; Zhang, Y.; Yu, W.; Shen, H.; Zhang, H.; Gu, N. Preparation and characterization of magnetite nanoparticles coated by amino silane. *Colloids Surfaces A Physicochem. Eng. Asp.* **2003**, *212*, 219–226. [[CrossRef](#)]
21. Zhu, X.M.; Wang, Y.X.; Leung, K.C.; Lee, S.F.; Zhao, F.; Wang, D.W.; Lai, J.M.; Wan, C.; Cheng, C.H.; Ahuja, A.T. Preparation and characterization of magnetite nanoparticles coated by amino silane. *Int. J. Nanomed.* **2012**, *7*, 953–964.
22. Mahmoudi, M.; Laurent, S.; Shokrgozar, M.A.; Hosseinkhani, M. Toxicity Evaluations of Superparamagnetic Iron Oxide Nanoparticles: Cell “Vision” versus Physicochemical Properties of Nanoparticles. *ACS Nano* **2011**, *5*, 7263–7276. [[CrossRef](#)] [[PubMed](#)]
23. Voinov, M.A.; Pagán, J.O.S.; Morrison, E.; Smirnova, T.I.; Smirnov, A.I. Surface-Mediated Production of Hydroxyl Radicals as a Mechanism of Iron Oxide Nanoparticle Biototoxicity. *J. Am. Chem. Soc.* **2010**, *133*, 35–41. [[CrossRef](#)] [[PubMed](#)]
24. Auffan, M.; Decome, L.; Rose, J.; Orsiere, T.; Meo, M.D.; Briois, V.; Chaneac, C.; Olivi, L.; Berge-Lefranc, J.L.; Botta, A. In vitro interactions between DMSA-coated maghemite nanoparticles and human fibroblasts: A physicochemical and cyto-genotoxic study. *Environ. Sci. Technol.* **2006**, *40*, 4367–4373. [[CrossRef](#)] [[PubMed](#)]
25. Karlsson, H.L.; Cronholm, P.; Gustafsson, J.; Moller, L. Copper oxide nanoparticles are highly toxic: A comparison between metal oxide nanoparticles and carbon nanotubes. *Chem. Res. Toxicol.* **2008**, *21*, 1726–1732.
26. Kunzmann, A.; Andersson, B.; Vogt, C.; Feliu, N.; Ye, F.; Gabrielsson, S.; Toprak, M.S.; Buerki-Thurnherr, T.; Laurent, S.; Vahter, M. Efficient internalization of silica-coated iron oxide nanoparticles of different sizes by primary human macrophages and dendritic cells. *Toxicol. Appl. Pharmacol.* **2011**, *253*, 81–93. [[CrossRef](#)]
27. Bondarenko, O.M.; Ivask, A.; Kahru, A.; Vija, H.; Titma, T.; Visnapuu, M.; Joost, U.; Pudova, K.; Adamberg, S.; Visnapuu, T. Bacterial polysaccharide levan as stabilizing, non-toxic and functional coating material for microelement-nanoparticles. *Carbohydr. Polym.* **2016**, *136*, 710–720. [[CrossRef](#)]
28. Mesarosova, M.; Ciampor, F.; Zavisova, V.; Koneracka, M.; Ursinyova, M.; Kozics, K.; Tomasovicova, N.; Hashim, A.; Vavra, I.; Krizanova, Z. The intensity of internalization and cytotoxicity of superparamagnetic iron oxide nanoparticles with different surface modifications in human tumor and diploid lung cells. *Neoplasma* **2012**, *59*, 584–597. [[CrossRef](#)]
29. Seinberg, L.; Volokhova, M. Metal-Based Core Nanoparticles, Synthesis and Use. WO2021/144006A1, 22 July 2020.
30. Volokhova, M.; Boldin, A.; Link, J.; Tsujimoto, M.; Stern, R.; Seinberg, L. Synthesis of Ni@SiO₂ and Co@SiO₂ nanomagnets by using calcium hydride as a reducing agent. *J. Mater. Res. Tech.* **2021**, *12*, 988–992. [[CrossRef](#)]
31. Lai, S.M.; Hsiao, J.K.; Yu, H.P.; Lu, C.W.; Huang, C.C.; Shieh, M.J.; Lai, P.S. Polyethylene glycol-based biocompatible and highly stable superparamagnetic iron oxide nanoclusters for magnetic resonance imaging†. *J. Mater. Chem.* **2012**, *22*, 15160–15167. [[CrossRef](#)]
32. Carroll1, M.R.J.; Woodward1, R.C.; House1, M.J.; Teoh, W.Y.; Amal, R.; Hanley, T.L.; Pierre1, T.G.S. Experimental validation of proton transverse relaxivity models for superparamagnetic nanoparticle MRI contrast agents. *Nanotech* **2010**, *21*, 35103. [[CrossRef](#)]

-
33. Duguet, E.; Vasseur, S.; Mornet, S.; Devoisselle, J.M. Magnetic Nanoparticles and Their Applications in Medicine. *Nanomed* **2006**, *1*, 157–168. [[CrossRef](#)] [[PubMed](#)]
 34. Aruoja, V.; Pokhrel, S.; Sihtmäe, M.; Mortimer, M.; Madler, L.; Kahru, A. Toxicity of 12 metal-based nanoparticles to algae, bacteria and protozoa. *Environ. Sci-Nano*. **2015**, *2*, 630–644. [[CrossRef](#)]